Measuring the Temperature of the Sun at 21cm

Lily Sun*
MIT Department of Physics
(Dated: April 7, 2026)

We use the MIT Medium Radio Telescope to measure the Sun's brightness temperature at 21 cm. By characterizing the telescope beam from azimuth and elevation scans, and applying an additional gain correction between the two polarization channels, we infer a solar brightness temperature of $467,000 \pm 26,000$ K and a beam width of $\theta_A = 2.74 \pm 0.05°$. Additional 2D and drift scans show that the beam is asymmetric and broader than an ideal Airy pattern, which dominates the systematic uncertainty. We interpret the measured brightness temperature as broadband free-free emission from the active solar atmosphere.

I. INTRODUCTION

The 21 cm band is central to radio astronomy. While it is best known for the neutral hydrogen spin-flip line which has been used extensively to trace galactic structure [1], observations at this wavelength can also detect broadband radio emission from astrophysical sources. In this experiment, we use the MIT Medium Radio Telescope (MRT) to measure the Sun's brightness temperature at 21 cm—the temperature of a blackbody with the same intensity at 21 cm.

Because the Sun is much smaller than the MRT beam, converting the measured antenna temperature into a solar brightness temperature requires an accurate beam model. We therefore measure the beam pattern using scans across the Sun and investigate deviations from an ideal Airy pattern. Using this beam pattern and an additional gain calibration, we infer the Sun's brightness temperature and discuss its physical origin in free-free emission from the solar atmosphere.

II. THEORY

II.1. The MRT Data Format

The MRT is an 18 ft diameter parabolic dish mounted on an azimuth-elevation (A, a) mount sitting atop the MIT Green Building. It consists of 2 channels, Ch0 and Ch1, which detect right-hand and left-hand circularly polarized light respectively. Since these are orthogonal polarizations, the total intensity is given by their sum.

We set the MRT to measure intensity in 512 frequency bins from 1419 MHz to 1421 MHz. For solar measurements, we average intensity across this narrow bandwidth to obtain the intensity at 21 cm, since we do not care about a specific 21 cm frequency but rather broadband radiation around 21 cm.

The MRT reports intensity in units of temperature, which is calibrated via a known noise diode (more details in Section III.2). Each spectrum comes from an integration time of $\tau = 2.097$ s. When we measure the temperature of any point, we use a total integration time $t > \tau$ to obtain multiple snapshots, then use the mean temperature across snapshots with its standard error.

Pointing the MRT directly at the Sun and recording for $t = 60$ s, we obtain a temperature of $T_{A,\mathrm{Ch0}} = 6173 \pm 7$ K and $T_{A,\mathrm{Ch1}} = 6070 \pm 6$ K. However, the temperature of the Sun is not simply the sum of these, because we must correct for the beam pattern due to diffraction.

II.2. MRT Beam Pattern

In this section we explain how we obtain the actual temperature of the Sun $T_\odot$ from the MRT's reading T_A.

Huygens' principle states that every point on a wavefront acts as a source of new wavelets. When light's path is blocked by a circular aperture, these wavelets cause the light to spread out (*diffract*), resulting in an Airy brightness pattern (Figure 1). We define the beam width θ_A as the full width at half of the maximum intensity (FWHM, see Figure 2). This scales with λ/D, making it a concern for radio astronomy as λ is relatively large.

Diffraction results in the MRT having a beam sensitivity pattern $P(\theta, \phi)$. This can be understood intuitively as follows—even if the MRT aperture is uniformly illuminated, diffraction through its circular aperture forms an Airy pattern which is focused at the focal plane, meaning the MRT has different sensitivity at different positions. For a circular aperture $P(\theta, \phi)$ should be an Airy pattern. For any $P(\theta, \phi)$, the beam width is still defined as the FWHM, and for the MRT the lab manual states that $\theta_A = 2.9°$.

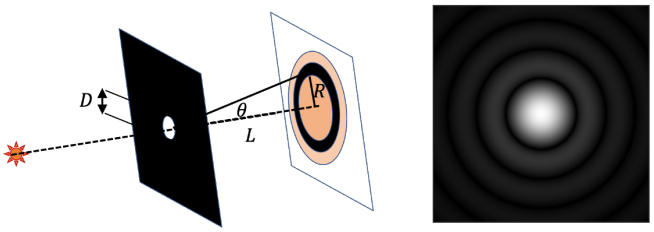

FIG. 1. Light through a circular aperture diffracts (left, image from [2]) resulting in an Airy pattern (right, image from [3]).

* xqsun@mit.edu

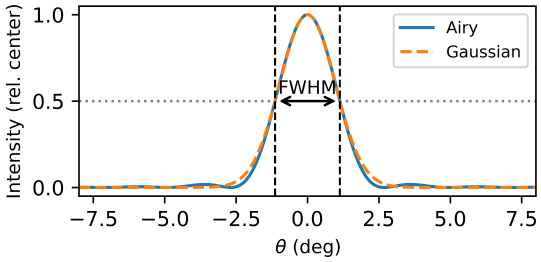

FIG. 2. Intensity against angle of Airy pattern. The beam width θ_A is the full width at half maximum, and we also show a Gaussian of the same θ_A.

The MRT measures the total power received, which is the true intensity multiplied by sensitivity at every point i.e. total power $= \iint T(\theta,\phi)P(\theta,\phi)d\Omega$ where for the Sun $T(\theta,\phi) = T_\odot$ within the Sun's radius ($\theta < 0.27°$) and $T = 0$ everywhere else. The MRT reports this number as T_A, the temperature of a *uniform* source that would provide this power, i.e. total power $= T_A \iint P(\theta,\phi)d\Omega$. Setting the powers equal, and knowing $P(\theta,\phi)$, one can then solve for $T_\odot$.

We assume $P(\theta,\phi)$ is Gaussian—as seen in Figure 2, a Gaussian and Airy with the same FWHM are very similar in the main lobe. We solve the integral analytically to obtain $\frac{T_A}{T_\odot} = \left[1 - \exp\left(-\frac{\theta_\odot^2}{2\sigma^2}\right)\right] \approx \frac{\Omega_\odot}{\Omega_A}$ i.e. T_A underestimates $T_\odot$ by the fraction of the MRT's beam width ($\Omega_\odot = 2\pi\sigma^2$ where $\theta_A = \sqrt{8\ln 2}\,\sigma$) that the Sun fills up. A back-of-the-envelope calculation using our T_A in *II* gives $\Omega_\odot/\Omega_A \approx 43$ and $T_\odot \approx 500,000$ K.

Instead of using the quoted value of θ_A, we will aim to experimentally measure this $P(\theta,\phi)$ by scanning across the Sun at different θ. This will give us $T_A(\theta) = \int T_\odot(\theta')P(\theta-\theta')d\theta'$, but we approximate the Sun to be a point source so that $T_A(\theta) \approx P(\theta)$. Our goal in the next section is to measure this beam pattern and use it to calculate the temperature of the Sun.

III. RESULTS

III.1. Azimuth and elevation scans of Sun

We first perform an azimuth scan of the Sun where we measure the temperature at each point from $\Delta A = -15°$ to $\Delta A = 15°$ from the Sun at intervals of 0.5° for $t = 30$ s each. To do this, we send a command file to the MRT that first points the MRT at the Sun then specifies an offset, re-pointing at the Sun after every measurement. We do the same for an elevation scan with $\Delta a = -15°$ to $\Delta a = 15°$. We convert the ΔA and Δa offsets to $\Delta\theta$ offsets where $\Delta\theta = \Delta a$ but $\Delta\theta = \Delta A \cos a$ (due to the way azimuth-elevation coordinates are defined, a change in azimuth at a higher elevation is a smaller change in angle than a change in azimuth at a lower elevation).

Figure 3 shows our results for the azimuth scan (top) and elevation scan (bottom). Each channel gives a profile which is a centered bell-shaped pattern. We first fit a Gaussian of the form $T_A = T_0 \exp\left(-\frac{(\theta-\mu)^2}{2\sigma^2}\right) + T_{bg}$ to each scan and channel's results to confirm that all four are centered bell-shaped patterns with comparable widths. We obtain four values of θ_A, one from each scan and channel (shown in the plots), and report the mean and error (conservatively, half of max-min) as $\theta_A = 2.76 \pm 0.04°$.

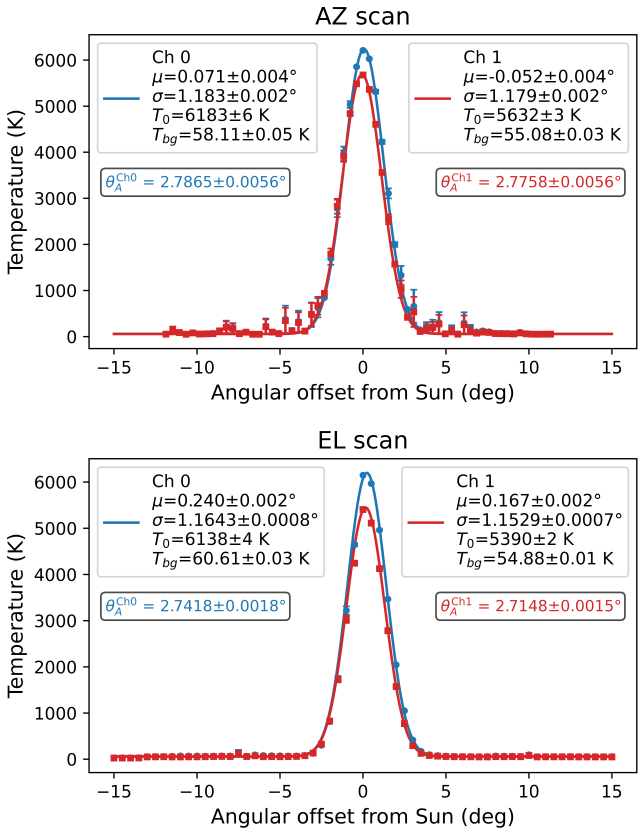

FIG. 3. Results from azimuth (top) and elevation (bottom) scan, separated by channel, each with its own Gaussian fit.

To obtain $T_\odot$, remembering that $T_A = T_{A,\mathrm{Ch0}} + T_{A,\mathrm{Ch1}}$, we add the per-channel temperatures before doing a Gaussian fit on the summed temperature (Figure 4). Then, using $\frac{T_0}{T_\odot} = \left[1 - \exp\left(-\frac{\theta_\odot^2}{2\sigma^2}\right)\right]$, we get $T_\odot^{AZ} = 470,800 \pm 1,400$ K and $T_\odot^{EL} = 441,230 \pm 430$ K.

From these results we notice two things. First, Ch1's T_A readings are consistently smaller than Ch0's by $\sim 10\%$, and second, there is a significant difference in θ_A and $T_\odot$ between the azimuth and elevation scans. We discuss the systematic error between channels in III.2 and the systematic error between scans in III.3.

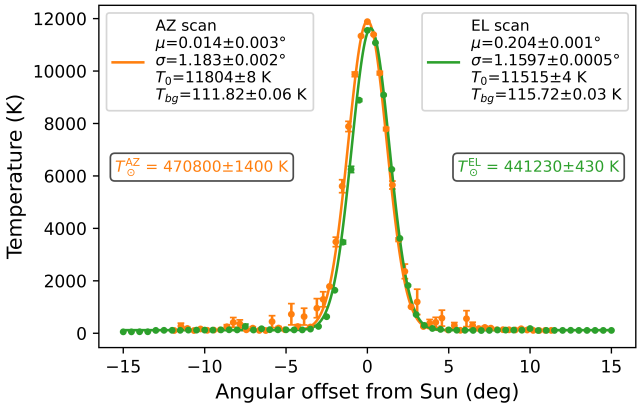

FIG. 4. Results from azimuth (top) and elevation (bottom) scan, summed over two channels. There is a systematic disagreement between azimuth and elevation scans.

III.2. Gain correction

Ch1's readings are consistently smaller than Ch0's readings, seemingly implying that the Sun is more right-hand circularly polarized. However, we know a priori that the Sun is unpolarized. Therefore, we will check the amplitude calibration of the MRT.

The MRT has an automatic amplitude calibration sequence. For each channel, it records the temperature of a blank point in the sky, then turns on that channel's noise diode creating a signal corresponding to a known temperature difference ($\Delta T_{\text{noise}} = 48.5$K for Ch0, $\Delta T_{\text{noise}} = 48.2$K for Ch1) and records the new temperature. The MRT then sets its units such that the temperature difference it reads is exactly ΔT_{noise}. This calibration sequence is done automatically before each of our measurements, but we do an additional calibration to see how far off we are from the ideal $G = \frac{\Delta T_{\text{actual}}}{\Delta T_{\text{noise}}} = 1$.

We point our telescope at the MRT's set calibration position and manually toggle the noise diodes as above ($t = 30$ s per setting), repeating five times to find $G_0 = 0.998 \pm 0.002$ and $G_1 = 0.910 \pm 0.004$. We note that Ch1's gain is indeed smaller than ideal by the previously observed $\sim 10\%$ (even at these low temperatures). We thus apply this systematic gain correction to each of our T_A to obtain corrected readings for each scan (Figure 5, $\theta_A = 2.74 \pm 0.05$) and see that the Ch0 and Ch1 within each scan look more similar. Summing these corrected values and fitting a Gaussian, we obtain $T_\odot^{AZ} = 493,000 \pm 1,700$ K and $T_\odot^{EL} = 440,060 \pm 880$ K (Figure 6) and thus an aggregate value of $T = 467,000 \pm 26,000$ K. Note that the gain correction has *increased* the disagreement between the two scans, even though it has corrected for the channel disagreement within each scan, likely due to the fitting.

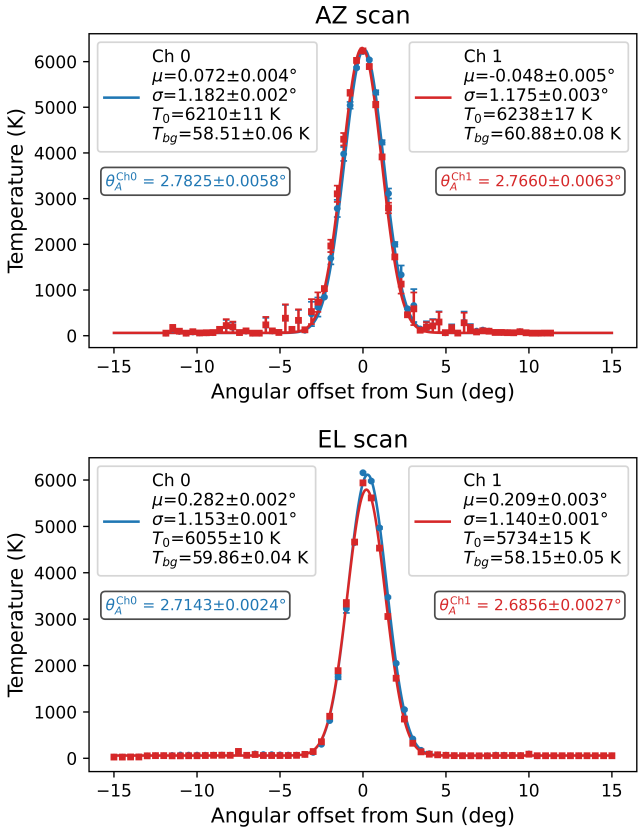

FIG. 5. Results from azimuth (top) and elevation (bottom) scan, gain-corrected. Ch0 and Ch1 are now more similar.

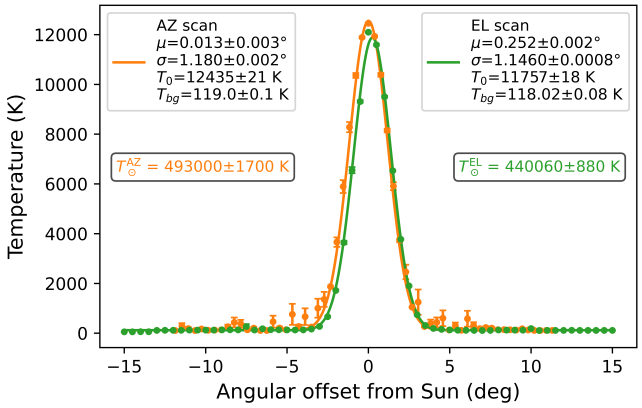

FIG. 6. Gain-corrected results for azimuth and elevation scans. There is still a systematic disagreement between scans.

III.3. Beam pattern

In this section, we further examine the beam pattern shape. First, given the systematic difference between the azimuth and elevation scans, we do a 2D grid scan of $\Delta A, \Delta a \in [-15°, 15°]$ at spacing 0.5° for $t = 10$s each, obtaining a 2D beam pattern (Ch0 plotted in Figure 7). We see that along the azimuth direction there is a greater

spread and more sidelobes. This confirms our previous finding that there is a systematic difference in beam pattern between the azimuth and elevation directions.

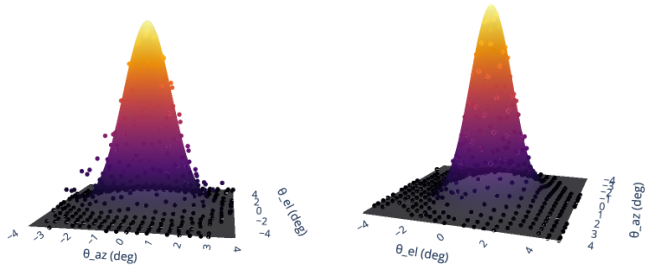

FIG. 7. Results from 2D scan for Ch0, showing azimuth (left) and elevation (right) directions.

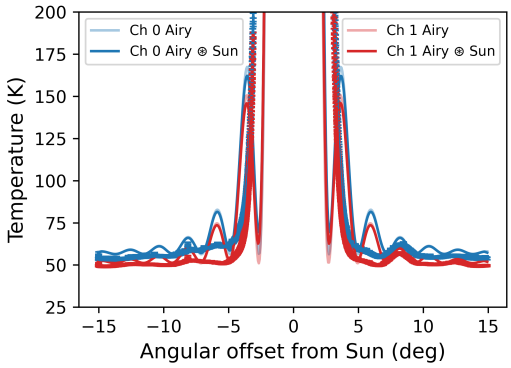

FIG. 8. Results from drift scan. The observed beam pattern is wider and has fewer sidelobes than the theoretical Airy and the theoretical Airy convolved with the Sun.

We also examine how Airy-like the beam pattern is. We do a "drift scan" of the Sun where we point the telescope at the Sun's position in the future and record continuously as it drifts across. This gives us 1 point of θ per integration time τ and thus a much higher spatial resolution to observe the beam pattern than our previous azimuth/elevation scans. Since we only have one snapshot per point, we estimate the error per point using the fractional error (standard deviation / mean, 1%) of the $\Delta A = \pm 15°$ temperatures from our azimuth scan.

Zooming in onto the sidelobe region, we plot the theoretical Airy pattern for a circular aperture using $\lambda = 21$ cm and $D = 18$ ft. We observe that the theoretical Airy pattern's main lobe is narrower and has more sidelobes than the observed beam pattern (light line). Convolving with the Sun's finite disk does not fix this discrepancy (dark line), supporting our earlier point-source approximation. Therefore, the main reason the beam pattern deviates from the theoretical Airy is likely due to the telescope's response. The Airy pattern results from a perfect circular aperture cutoff. However, if the MRT's sensitivity decreases towards the edges, this would result in a less sudden cutoff and thus fewer sidelobes in the beam pattern, as well as a broader beam since a tapering of sensitivity effectively uses a smaller beam width, which are both what we observe.

From our drift scan we can also perform the gain-correction and get $T_\odot^{drift} = 453,090 \pm 220$ K. This compares to our previous value of $T_\odot^{AZ,EL} = 467,000 \pm 26,000$ K but without the large systematic error between the scans. However, this drift scan underestimates the error due to its assumption of a circular beam pattern which we know is not true, and so a better report for the temperature of the Sun would still be from our azimuth and elevation scans $T_\odot^{AZ,EL} = 467,000 \pm 26,000$ K.

IV. INTERPRETATION OF RESULTS

The 21 cm radiation we are measuring is *bremsstrahlung* emission—free electrons in the Sun's atmosphere are scattered by charged particles and this change in momentum causes emission of broadband photons.

The brightness temperature $T_B \approx 467,000$ K is related to but not necessarily equal to the actual electron temperature. If the plasma is optically thick, the photons will be in thermodynamic equilibrium ($T_B \approx T_e$) with electrons as photons are rapidly emitted, absorbed and re-emitted at the electron local temperature. However if the plasma is optically thin, then the photon energy distribution is not necessarily that of a blackbody at T_B as they are *bremsstrahlung* photons. We likely measure some intensity contribution from both optically thick and thin areas, so our T_B does not necessarily relate to electron temperature. Lastly, the photons we measured likely originated from the solar atmosphere rather than the surface, because nearer the Sun's surface it is too optically dense for 21 cm radiation to pass through.

Our results are significantly higher than past measurements of the temperature of the Sun—most sources measure a quiet Sun of $T_B \approx 50,000$ K [4, 5]; Bastian and Dulk [6] found a variation of up to 200,000 K in 1981. Our measurements were taken in March 2026 which is after a solar maximum in late 2024, and radio intensity is a lot higher for an active Sun [7].

V. CONCLUSION

We measured the Sun's brightness temperature at 21 cm to be $T_\odot = 467,000 \pm 26,000$ K using the MRT. The dominant uncertainty is systematic and arises from the telescope beam, which is asymmetric and broader than an ideal Airy pattern; an additional gain correction was also needed to reconcile the two channels. Despite these instrumental limitations, the inferred brightness temperature is much higher than that of the quiet Sun and is consistent with enhanced free-free emission from an active solar atmosphere.

ACKNOWLEDGMENTS

We thank Liam Sheldon for collaboration on collecting data, 8.13 instructors and TAs for their guidance, and the team involved in maintaining the MRT.

---

[1] W. N. Christiansen and J. V. Hindman, The Observatory **72**, 149 (1952).
[2] Physics Bootcamp, "Section 11.8: Circular aperture and angular resolution," https://www.physicsbootcamp.org/section-circular-aperture-and-angular-resolution-light.html (n.d.), accessed: 2026-04-06.
[3] Wikipedia contributors, "Airy disk — wikipedia, the free encyclopedia," https://en.wikipedia.org/wiki/Airy_disk (2026), accessed: 2026-04-06.
[4] W. N. Christiansen and J. A. Warburton, Australian Journal of Physics **8**, 474 (1955).
[5] Progress In Electromagnetics Research Letters **85**, 17 (2019).
[6] T. S. Bastian and G. A. Dulk, in *Solar and Stellar Coronal Structure and Dynamics*, edited by R. C. Altrock (1988) pp. 386–391.
[7] C. Ho, S. Slobin, A. Kantak, and S. Asmar, Interplanetary Network Progress Report **42-175**, 1 (2008).